Article

Origin of Selectivity Switch in Fischer#Tropsch Synthesis over Ru and Rh from First-Principles Statistical Mechanics Studies

Jia Chen, and Zhi-Pan Liu

J. Am. Chem. Soc., **2008**, 130 (25), 7929-7937 • DOI: 10.1021/ja7112239 • Publication Date (Web): 29 May 2008

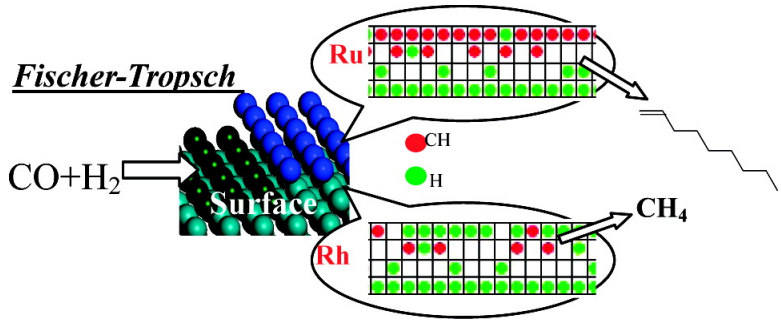

More About This Article

Additional resources and features associated with this article are available within the HTML version:

- Supporting Information
- Access to high resolution figures
- Links to articles and content related to this article
- Copyright permission to reproduce figures and/or text from this article

View the Full Text HTML

J|A|C|S
ARTICLES

Published on Web 05/29/2008

Origin of Selectivity Switch in Fischer−Tropsch Synthesis over Ru and Rh from First-Principles Statistical Mechanics Studies

Jia Chen and Zhi-Pan Liu*

Shanghai Key Laboratory of Molecular Catalysis and Innovative Materials, Department of Chemistry, Fudan University, Shanghai, China 200433

Received December 19, 2007; E-mail: zpliu@fudan.edu.cn

Abstract: For its unique position in chemical industry, Fischer−Tropsch (FT) synthesis has been a hot subject in heterogeneous catalysis. Due to its great complexity in product distribution, it remains unclear how to maximally convert syngas to long-chain hydrocarbons. By combining extensive DFT calculations with grand canonical Monte Carlo simulations, this work examines the key elementary steps in FT synthesis over Ru and Rh surfaces, including CO dissociation, C/C coupling, and hydrogenations. The origin of the relationship between activity and selectivity of catalysts is revealed based on the calculated reaction rate at working temperatures, in which the catalytic role of surface steps as the center of accumulating surface CH_x species is highlighted. This theoretical work demonstrates that the ability to dissociate CO under carbon-rich conditions is the key requirement for a good FT catalyst. The RC + C (R = alkyl or H) pathway occurring at surface steps may be a general mechanism for FT chain propagation on transition metals.

1. Introduction

Fischer−Tropsch (FT) synthesis, which converts syngas (CO and H_2) into high molecular weight hydrocarbons, is increasingly attracting global interests. As a synthetic route to make fuels and valuable organic compounds from natural gas or coal,[1,2] Fischer−Tropsch technology has a unique position in chemical industry with huge economic incentives. It was established by numerous experimental studies[3] that the FT activity of group VIII metals varies dramatically, which decreases in an order of Ru, Fe, Co, Rh, Ni, Pd, and Pt. Despite the huge efforts devoted to elucidate the FT mechanism, some key issues remain elusive. In particular, it is still not clear that why the earlier metals such as Ru selectively produce very high molecular weight hydrocarbons up to C_{20}, while the latter metals such as Rh and Ni mainly yield methane, the undesired product in the FT process. As the selectivity issue lies at the heart of FT technology, a better atomic-level understanding is urgently required.

The general mechanism of the FT process can be described as follows. Initially, CO adsorbs and dissociates into adsorbed C and O atoms on catalysts. The dissociating product O can be efficiently removed by H to form water that desorbs at reaction conditions. The adsorbed C can recombine with H to yield various C_1 hydrocarbons (CH_x, $x = 0, 1, 2, 3$).[4] Then the chain growth starts via the C/C coupling, which competes with the chain termination via the hydrogenation. Good FT catalysts selectively produce long-chain hydrocarbons that are mainly α-olefin and linear paraffin, and methane is the major byproduct.[2] The chain growth can be well accounted by a simple polymerization mechanism with C_1 species as the building monomer since the molecular weights of hydrocarbon products follow the Anderson−Schulz−Flory distribution.[5]

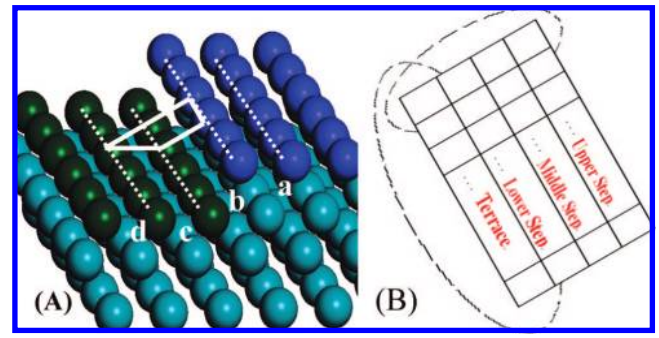

Figure 1. (A) Structure of the surface steps as represented by a Ru surface. Circulated by the solid line is a B_5 stepped site, which contains two step-edge atoms and three atoms at lower terraces. (B) Two-dimensional lattice model in MC simulations with periodical boundary conditions (indicated by the dashed lines). The upper step, middle step, and lower step correspond to a-b, b-c, and c-d areas in (A), and the other exposed sites in (A) belong to terraces.

Microscopically, the mechanism of CO dissociation on transition metals was recently resolved.[6–9] Based on both density functional theory (DFT) calculations [6,7] and experimental observations,[8,9] metal monatomic steps, the so-called B_5 site (Figure 1A), were shown to be the active site for CO dissociation. Consequently, in the FT process the surface carbides would

(1) Khodakov, A. Y.; Chu, W.; Fongarland, P. *Chem. Rev.* **2007**, *107*, 1692.
(2) Schulz, H. *Appl. Catal., A* **1999**, *186*, 3.
(3) Vannice, M. A. *J. Catal.* **1977**, *50*, 228.
(4) Hilmen, A. M.; Schanke, D.; Hanssen, K. F.; Holmen, A. *Appl. Catal., A* **1999**, *186*, 169.
(5) Van Der Laan, G. P.; Beenackers, A. A. C. M. *Catal. Rev. -Sci. Eng.,* **1999**, *41(3−4)* , 255.
(6) Hammer, B. *Phys. Rev. Lett.* **1999**, *83*, 3681.
(7) Liu, Z.-P.; Hu, P. *J. Am. Chem. Soc.* **2003**, *125*, 1958.
(8) Zubkov, T.; Morgan, G.A., Jr.; Yates, G.T., Jr. *Chem. Phys. Lett.* **2002**, *362*, 181.
(9) Mavrikakis, M; Beaumer, M; Freund, H.-J.; Noskov, J. K. *Catal. Lett.* **2002**, *81*, 153.

first appear at the lower steps while the O emerges at the upper steps.[10] Water formation and O removal were studied recently by DFT calculations, showing that the O removal is very efficient via OH−OH coupling, i.e., $O + O + 3H \rightarrow O + OH + 2H \rightarrow 2OH + H \rightarrow H_2O + OH$.[10,11] The chain growth mechanism, in spite of its paramount importance, is still highly controversial.[12–16] Perhaps the best-known mechanism proposed is a $CH_2 + CH_2R$ pathway with the adsorbed CH_2 species as the building monomer. [2,17] However, no direct experimental evidence proved the $CH_2 + CH_2R$ mechanism, and the available theoretical results were all against this mechanism since (i) surface CH_2 is unstable compared to surface C and CH species and (ii) the prototypical chain-growth reaction $CH_2 + CH_3$ has high energy barriers on metals. Other alternative mechanisms have been proposed.[14] Our previous work based on a DFT-slab approach revealed that monatomic steps are generally more active than terraces for C/C coupling reactions on Ru.[18] In the work, a $CR + C \rightarrow RC-C$ (R = H or alkyl) mechanism was suggested for the chain growth, in which the C atom locates at the lower steps and the CR sits at the upper steps.

Understanding the origin of the selectivity is now a top priority in FT technology. It is not difficult to understand why Pd and Pt are not good FT catalysts since CO dissociation on them is prohibitively difficult without promoters.[6,19] It is however quite puzzling that the metals such as Ru and Rh have rather distinct selectivities. These two metals are neighbors in the periodic table, and both can convert CO to hydrocarbons. It appears that earlier metals such as Ru, Fe, and Co generally prefer to produce long-chain hydrocarbons, while the late metals such as Ni and Rh produce methane dominantly. To fully resolve these puzzles, one has to compare the reaction rate under realistic conditions, which was, however, a formidable task for theoreticians for years. This is because the first-principles calculations only give the energetics at zero Kelvin and zero bar, while the mean-field microkinetics with a large number of empirical parameters often lack atomic-level understanding of the reactions. Recently the first-principles statistical mechanics demonstrated great potentials in tackling complex surface reactions. Reuter at al. carried out a DFT-based kinetic Monte Carlo (MC) simulation to describe the oxidation of CO over a $RuO_2(110)$ surface.[20] With an equilibrium assumption, ammonia synthesis on a supported nanoparticle Ru catalyst was examined by Honkala et al. using a one-dimensional lattice grand canonical ensemble Monte Carlo model together with DFT calculations.[21] They obtained a set of distributions for various reaction intermediates over the active site of Ru and predicted reasonably the reaction rates at industrial conditions.

Inspired by these works, here we combine Monte Carlo simulation with extensive DFT calculations to provide an atomic-level description of FT kinetics on Ru and Rh. Due to the complexity of the FT process where the exact nature of C/C pairs under realistic conditions are critical, we develop a two-dimensional lattice model for a grand canonical ensemble Monte Carlo simulation that includes both surface defects and terraces. Using the equilibrium assumption, we show how the selectivity is switched from long-chain hydrocarbons to methane on going from Ru to Rh. Deeper insights into the chain growth mechanism are also obtained.

2. Modeling and Computational Details

2.1. DFT Calculation Setups. All total energy density functional theory calculations were first carried out with the SIESTA package[22] using numerical orbital atomic basis sets and Troullier−Martins norm-conserving scalar relativistic pseudopotentials.[22–24] This localized-orbital method is particularly efficient to map out the potential energy surface, to calculate the vibrational frequencies, the lateral interaction, and the reaction barrier, where the accuracies are generally good and comparable to the plane-wave method. To obtain more accurate energetics such as adsorption energy for MC simulation, the final adsorption energies of the adsorbates were calculated with the VASP package, in which the basis sets are expanded with plane waves[25,26] up to a kinetic cutoff energy of 400 eV and the valence electrons of elements are treated by Vanderbilt ultrasoft pseudopotentials.[27,28] The exchange-correlation functional utilized is the local-density-approximation with generalized gradient correction.[29,30] In SIESTA, the double-ξ plus polarization basis (DZP) set was employed for basis set expansion. The orbital-confining cutoff radii were determined from an energy shift of 0.01 eV. The energy cutoff for the real space grid used to represent the density was set as 150 Ry. The vibrational frequencies of adsorbates were obtained by numerical finite displacement method.

In DFT calculations, all the metal surfaces are modeled with four-layer slabs with the top two layers being relaxed. The terrace of Ru and Rh are modeled by $p(3 \times 3)$ Ru(0001) and Rh(111) slabs, respectively. The stepped Ru surface is modeled by $p(5 \times 3)$ and $p(5 \times 2)$ slabs with the top two rows of surface atoms being removed, which is the typical approach used to study the monatomic steps of Ru.[6,18,21] The stepped Rh surface is modeled by a Rh(322) slab, where each (100) step is separated by four rows of (111) surface sites. Monkhurst−Pack k-point sampling with $0.05 \times 2\pi$ $Å^{-1}$ spacing in a reciprocal lattice was used for all of the calculations.

Transition states (TSs) of the catalytic reactions were searched by the constrained minimization method.[7,31] All degrees of freedom except for the constrained reaction coordinate were relaxed. The TSs are identified when (i) the forces on the atoms vanish and (ii) the energy is a maximum along the reaction coordinate, but a minimum with respect to all of the other degrees of freedom. We have checked the energy barriers of key reactions such as CO dissociation, which ensures that the results of SIESTA are consistent with those from the plane-wave methods.

2.2. Thermodynamics. At chemical equilibrium, the chemical potentials (μ) of the H and C element in the system are pinned by the gas phase molecules, hydrogen and methane. We obtained the chemical potential of H and C based on the standard thermodynamics data, e.g., from *NIST Chemistry WebBook* (http://webbook.nist.gov/chemistry/). The detailed equations to derive the chemical

(10) Gong, X.-Q.; Raval, R.; Hu, P. *Surf. Sci.* **2004**, *562*, 247.
(11) Gong, X.-Q.; Raval, R.; Hu, P. *Mol. Phys.* **2004**, *102*, 1993.
(12) (a) Brady, R.; Pettit, R. *J. Am. Chem. Soc.* **1981**, *103*, 1287. (b) Turner, M. L.; Marsih, N.; Mann, B. E.; Quyoum, R.; Long, H. C.; Maitlis, P. M. *J. Am. Chem. Soc.* **2002**, *124*, 10456.
(13) Ge, Q.; Neurock, M.; Wright, H. A.; Srinivasan, N *J. Phys. Chem. B* **2002**, *106*, 2826.
(14) Ciobica, I. M.; Kramer, G. K.; Ge, Q.; Neurock, M.; van Santen, R. A. *J. Catal.* **2002**, *212*, 136.
(15) Ciobica, I. M.; van Santen, R. A. *J. Phys. Chem. B* **2002**, *106*, 6200.
(16) Au, C.-T.; Ng, C.-F.; Liao, M.-S. *J. Catal.* **1999**, *185*, 12.
(17) Schulz, H.; Claeys, M. *Appl. Catal., A* **1999**, *186*, 91.
(18) Liu, Z.-P.; Hu, P. *J. Am. Chem. Soc.* **2002**, *124*, 11568.
(19) Liu, Z.-P.; Hu, P. *J. Chem. Phys.* **2001**, *114*, 8244.
(20) Reuter, K.; Frenkel, D.; Scheffler, M. *Phys. Rev. Lett.* **2004**, *93*, 116105.
(21) Honkala, K.; et al. *Science* **2005**, *307*, 555.
(22) Soler, J. M.; Artacho, E.; Gale, J. D.; Garcia, A.; Junquera, J.; Ordejon, P.; Sanchez-Portal, D. *J. Phys.: Condens. Matter* **2002**, *14*, 2745.
(23) Junquera, J.; Paz, O.; Sanchez-Portal, D.; Artacho, E. *Phys. Rev. B* **2001**, *64*, 235111.
(24) Troullier, N.; Martins, J. L. *Phys. Rev. B* **1991**, *43*, 1993.
(25) Kresse, G.; Hafner, J. *Phys. Rev. B* **1993**, *47*, 558.
(26) Kresse, G.; Hafner, J. *Phys. Rev. B* **1994**, *49*, 14251.
(27) Kresse, G.; Hafner, J. *J. Phys.: Condens. Matter* **1994**, *6*, 8245.
(28) Vanderbilt, D. *Phys. Rev. B* **1990**, *41*, 7892.
(29) Perdew, J. P.; Chevary, J. A.; Vosko, S. H.; Jackson, K. A.; Penderson; M, R.; Singh, D. J.; Fiolhais, C. *Phys. Rev. B* **1992**, *46*, 6671.
(30) Perdew, J. P.; Wang, Y. *Phys. Rev. B* **1992**, *45*, 13244.
(31) Wang, C.-M.; Fan, K.-N.; Liu, Z.-P. *J. Am. Chem. Soc.* **2007**, *129*, 2642.

potenital of the gas phase molecule at finite T and P can be found in previous publications.[21,32–34]

To convert DFT total energy (E_{DFT}) to free energy F at the finite temperatures and pressures, the following thermodynamic formula are applied to the adsorbed species on surfaces:[33,34]

$$F = E_{DFT} + ZPE - TS \quad (1)$$

$$s = \frac{\partial F}{\partial T}|_V = k_B \ln q_{vib} + k_B T \frac{\partial \ln q_{vib}}{\partial \ln T} \approx k_B \ln q_{vib} \quad (2)$$

$$q_{vib} = \prod_{i=1}^{3n} (1 - \exp(-h\nu_i/k_B T))^{-1} \quad (3)$$

where ZPE is the zero-point energy, q_{vib} is the vibration partition function, and ν_i is the vibrational frequency of adsorbates.

2.3. Monte Carlo Modeling. It is known that CO dissociation occurs at the B_5 stepped sites on Ru and Rh (as illustrated in Figure 1), and our previous work also showed that the B_5 stepped sites are also much more active than the terrace sites for C/C coupling on Ru.[18] These two facts prompt us to establish a general model that represents the whole B_5 sites with the aim to describe the chemistry in the FT process. In this work, we developed a two-dimensional lattice model that includes four rows of sites, namely, the upper step, the middle step, the lower step, and the terrace, as shown in Figure 1. Each row contains 50 sites with periodical boundary conditions being imposed. This two-dimensional model is essential, not least because our DFT calculations show that C_1 intermediates such as C and CH can adsorb not only at the upper and lower steps but also strongly at the fourfold hollow site of the middle steps that was largely overlooked previously. As the stepped sites are the reaction center, the terrace sites here are only represented by one row of lattice (see Figure 1), which are mainly used as the reservoir of adsorbed species and simultaneously allow the diffusion of species between the upper steps and the lower steps.

In our Monte Carlo simulation, we assume H atoms and all C_1 species (C, CH, CH_2, CH_3, CH_4(g)) reach equilibrium before any C/C chain growth starts. This is a good assumption in general, in particular for the poor FT catalyst where the C/C coupling is slow. It may also be quite reasonable at the beginning of FT conversion when hydrogen atoms are abundant on surfaces considering that hydrogen has the lowest diffusion energy barriers.[35] In the section 3.6, we will discuss this equilibrium assumption in detail. We did not consider CO adsorption and desorption in the MC simulation because they are fast reversible steps at FT conditions (e.g., 600 K), which do not compete with adsorbed H atoms and C_1 species for surface sites.

Grand canonical ensemble Monte Carlo[36] was employed to achieve the thermodynamic equilibrium. In the MC simulation, the following five reactions were taken into account for the system to reach equilibrium:

$$\frac{1}{2}H_2 + \square \rightleftarrows H^*$$

$$C^* + H^* \rightleftarrows CH^* + \square$$

$$CH^* + H^* \rightleftarrows CH_2^* + \square$$

$$CH_2^* + H^* \rightleftarrows CH_3^* + \square$$

$$CH_3^* + H^* \rightleftarrows CH_4 + 2\square$$

Here $\square$ represents an unoccupied surface site (vacancy) and X* represents the adsorbed species. According to the principle of microscopic reversibility, if one process can occur, the reverse one is allowed in our simulation. In this work, we choose a typical FT synthesis condition to carry out the simulation: the total pressure p = 2.0 MPa, the mol ratio H_2/CO = 2, and the selectivity to C_1 product methane is 10%. The total chemical potential of all C_1 intermediates, namely, C, CH, CH_2, and CH_3, can then be derived by the equilibrium condition. We also carefully tested the convergence of the Monte Carlo simulation with respect to the simulation steps. Our final statistical result is the average of 100 million (10^8) samplings at equilibrium that is achieved after 1 billion (10^9) Monte Carlo iterations.

Table 1. Calculated Adsorption Energies and Adsorption Site (See Figure 1) of H and C_1 Species[a]

	H	C	CH	CH_2	CH_3
Ru: upper	−3.08 (hcp)	−7.99 (hcp)	−11.58 (hcp)	−13.70 (hcp)	−16.70 (hcp)
middle	−3.14 (eb)	−8.18 (fh)	−11.26 (fh)	−13.81 (eb)	−16.42 (top)
lower	−2.93 (hcp)	−7.59 (hcp)	−10.90 (hcp)	−13.44 (hcp)	−16.36 (fcc)
terrace	−3.10 (fcc)	−8.03 (hcp)	−11.17 (hcp)	−13.76 (hcp)	−16.65 (hcp)
ΔE(t−s)	−0.04	−0.15	−0.41	−0.05	−0.05
Rh: upper	−3.01 (hcp)	−7.72 (hcp)	−10.96 (hcp)	−13.46 (hcp)	−16.44 (hcp)
middle	−3.03 (eb)	−8.17 (fh)	−11.05 (fh)	−13.66 (eb)	−16.43 (top)
lower	−2.96 (hcp)	−7.54 (hcp)	−10.92 (hcp)	−13.38 (hcp)	−16.13 (hcp)
terrace	−3.03 (fcc)	−7.71 (hcp)	−10.97 (hcp)	−13.46 (fcc)	−16.38 (fcc)
ΔE(t−s)	0.00	−0.46	−0.08	−0.20	−0.06

[a] The adsorption energy is referenced to the gas phase carbon and hydrogen atoms. ΔE(t−s) is the maximum energy difference for a species moving from the terrace to the stepped sites. eb: edge-bridge. fh: fourfold hollow. All energies are in eV.

The reaction rate of surface reactions is calculated according to the rate equation. For example, the rate equation of an AB → A + B reaction can be written as eq 4. We assume the preexponential factor at 300 K being 10^{13}, and it scales to different temperatures by T/300. The E_a is calculated from DFT, and the coverage θ is obtained directly from MC simulation.

$$r = \frac{T}{300} \times 10^{13} \times e^{-E_a/RT} \times \theta \quad (4)$$

3. Results

3.1. Adsorption of Reaction Intermediates: Energetics and Frequencies. Using DFT, we have calculated the potential energy surface of the reaction intermediates, namely the H atom, the C atom, CH, CH_2, and CH_3 on Ru and Rh. The calculated adsorption energies at the most stable sites for them at the upper, middle, and lower steps and terraces are listed in Table 1. Two general trends for the adsorption can be identified. (i) The adsorption energies of adsorbates on Ru are generally larger than their counterparts on Rh. This is consistent with the general consensus that Ru is a more active metal than Rh because the d-states of Ru being closer to Fermi level can form a stronger covalent bonding with adsorbates.[37,32] There is also a special case, i.e., the C atom adsorption on Rh steps, where the adsorption energy is particularly large, being almost identical to that on Ru. We found that, in this case, the C atom almost falls into the hollow site of the Rh steps forming one more bonding with a subsurface Rh atom. (ii) On both metals, the stepped sites including the upper steps and the middle steps can bond adsorbates more strongly compared to the terrace sites. This is not surprising as these sites with less coordinated metal atoms (step-edge atoms) have more active d-states, which can form better covalent bonding with adsorbates.[6,32] By comparing the maximum energy difference for a species migrating from terraces to steps (ΔE(t−s)), we can see that H atoms have quite flat potential energy surfaces on both surfaces, while the highly unsaturated C and CH prefer the stepped sites. There is a large

(32) Liu, Z.-P.; Jenkins, S. J.; King, D. A. *J. Am. Chem. Soc.* **2004**, *126*, 10746.
(33) Bollinger, M. V.; Jacobsen, K. W.; Norskov, J. K. *Phys. Rev. B* **2003**, *67*, 085410.
(34) Loffreda, D. *Surf. Sci.* **2006**, *600*, 2103.
(35) Nilekar, A. U.; Greeley, J.; Mavrikakis, M. *Angew. Chem., Int. Ed.* **2006**, *45*, 7046.
(36) Landau, D. P.; Binder, K. *A Guide to Monte Carlo Simulations in Statistical Physics*; Cambridge University Press; Cambridge, 2000.
(37) Hammer, B.; Norskov, J. K. *Adv. Catal.* **2000**, *45*, 71.

Table 2. Vibrational Frequencies and Zero-Point Energies of Adsorbates

	Ru/cm^{-1}	ZPE/eV	Rh/cm^{-1}	ZPE/eV
H	1005, 1112, 1221	0.21	919, 1160, 1180	0.20
C	572, 581, 613	0.11	567, 594, 610	0.11
CH	486, 497, 647, 711, 720, 3030	0.38	521, 543, 639, 706, 719, 3004	0.38
CH_2	325, 344, 408, 534, 6247, 776, 1325, 2847, 2949	0.63	295, 436, 501, 571, 598, 790, 1289, 2865, 2965	0.64
CH_3	365, 394, 422, 462, 509, 620, 1187, 1217, 1298, 2529, 2631, 2658	0.89	323, 349, 438, 459, 523, 554, 1198, 1210, 1237, 2572, 2619, 2634	0.85

increase of adsorption energy for CH on Ru and for C on Rh on going from terraces to steps.

Next, we calculated the vibrational frequencies for all the adsorbates using DFT, which were used to compute the zero-point energies (ZPEs) and the entropy contributions at finite temperatures. In Table 2, we list the calculated vibrational frequencies of the adsorbed species on Ru and Rh terraces together with the calculated zero-point energies. It shows that the ZPEs of the adsorbates on Ru and Rh are essentially the same.

3.2. Lateral Interaction between Adsorbates. Under catalytic conditions, the surface of the catalyst must be covered with different species at a finite coverage. This implies that the lateral interaction among species has an important contribution to the total free energy of the system. In MC simulations, this must be taken into account in order to predict correctly the distribution of species. Because of the intrinsic complexity of the many-body problem, we have simplified our treatment by representing the lateral interaction between species (H, C, CH, CH_2, CH_3) with a pairwise model. As shown by equation4, the lateral interaction can be calculated within DFT as the energy difference between the coadsorption system and the individual adsorbed systems.

$$\Delta E_{\text{late}} = E_{\text{AB}} + E_{\text{surface}} - E_{\text{A}} - E_{\text{B}} \quad (5)$$

Even in the pairwise model, there are still a great number of possibilities of adsorbate−adsorbate pairs mathematically. In a systematic manner, we classified the possible combinations into three categories according to the number of surface atoms being shared by the neighboring adsorbates. The more the atoms are being shared by the two adsorbates, the larger the repulsive interaction between them. The physical origin of this was well-addressed previously as a so-called surface-mediated bonding competition effect.[38,37,32] In this work, we omitted the lateral interaction between non-neighboring adsorbates where no surface atoms are shared. The magnitude of such long-range interactions is typically small, i.e., below 0.05 eV. We explicitly calculated the lateral interaction involving two metal atoms being shared, which will induce the largest repulsive effects. These may include the interaction between two neighboring adsorbates at the middle steps (Figure 2 top panel) and the interaction between an upper-step adsorbate and a middle-step adsorbate (Figure 2 middle panel). For the lateral interaction involving only one surface atom being shared, there are in total three cases, where both adsorbates locate (i) at the upper steps, (ii) at the lower steps, and (iii) at the terraces (as shown in Figure 2 bottom panel). For the three situations, we found that the magnitudes of the interaction for the same pair of adsorbates are similar, and thus we represented the lateral interaction of this type using

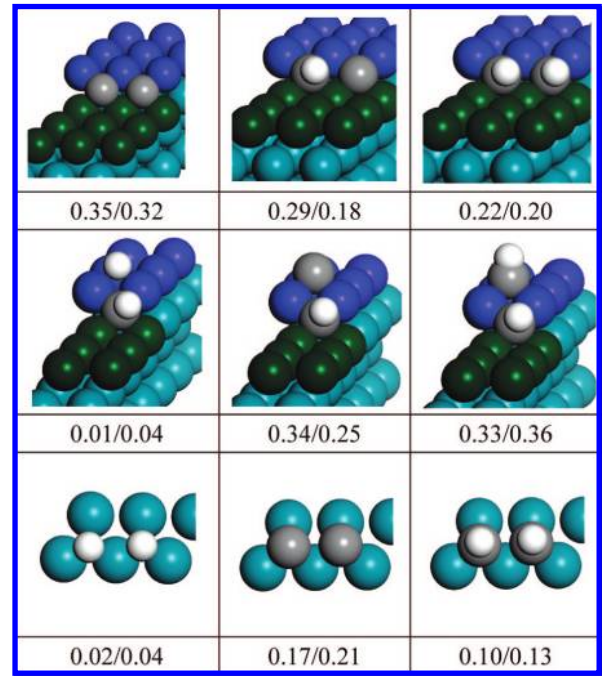

Figure 2. Pairwise model for calculating lateral interactions between two neighboring adsorbates. These representative results are taken from the optimized structures on Ru. The energy values (unit: eV) beneath the figures are the lateral interaction on Ru and Rh, respectively.

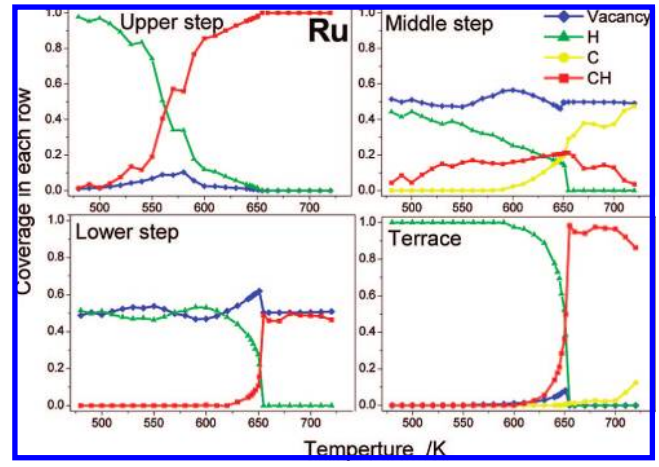

Figure 3. Monte Carlo simulated surface composition on Ru.

the lateral interaction at the terraces for simplicity. Finally, there is a special case where two neighboring adsorbates are too close in space, that is, one adsorbate at the lower steps and another one at the middle steps. Due to the large repulsion incurred, we do not allow for this situation in the MC simulation.

3.3. Surface Composition from MC Simulation. With the above data, we were able to perform Monte Carlo simulations to study the surface composition of Ru and Rh. We have summarized the MC simulated surface compositions in Figures 3 and 4 for Ru and Rh, respectively, where the coverage in each row is plotted against the temperature. Our Monte Carlo simulations show that H, C, and CH are the most common species on both Ru and Rh surfaces under FT synthesis conditions, inconsistent with experimental facts.[39] The coverages of CH_2 and CH_3 are much lower than the

(38) Bleakley, K.; Hu, P. *J. Am. Chem. Soc.* **1999**, *121*, 7644.

(39) Somorjai, G. A. *Introduction to Surface Chemistry and Catalysis*; John Wiley & Sons: New York, 1994.

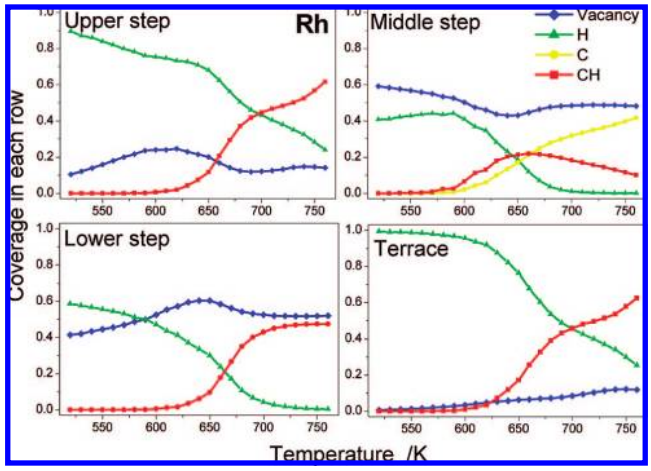

Figure 4. . Monte Carlo simulated surface composition on Rh

dominant species by at least 1 order of magnitude at all temperatures investigated.

At low temperatures, the surfaces are hydrogen-rich (e.g., below 520 K). At high temperatures, CH is almost the only surface species except at the middle step where C is present at the fourfold hollow site. Because CH strongly prefers the upper step hcp site on Ru, the upper step is filled up with CH quickly with the increase of temperature, while this does not happen on Rh. On both metals, the middle step is maximally half-filled even at high temperatures, not least because the large lateral repulsion between two neighboring C or CH species. The lower steps always have the highest concentration of vacant sites since the lower steps have the lowest binding ability (Table 1), and there is also large through-space repulsion in the presence of middle-step adsorbates. Even at high temperatures, the lower steps remain at least 50% vacant. This implies that CO can always adsorb at the lower steps and wait for dissociation until the upper step site is empty.

In Figure 5 we further compare the equilibrium snapshots of the Ru and Rh surface at 630 K. At this temperature, Ru and Rh are very different in surface species at the stepped sites, although their terraces are similarly dominated by H. On both surfaces, the lower steps are largely unoccupied. The upper steps are mostly occupied by CH on Ru but H on Rh. At the middle steps, C or CH species generally prefer to avoid each other, which yield a rather regular pattern with one vacancy or one H between them. It should be pointed out that the stepped sites are not totally blocked despite the high adsorption energy of C and CH at the middle steps. The self-poisoning is prevented by the lateral interaction. If the middle steps were fully occupied, there would be a large repulsive interaction within the same row and the bondings of the upper- and the lower-step species would also be significantly weakened.

3.4. CO Dissociation and Activity of FT Catalysts. The grand canonical Monte Carlo simulation results above outline the surface composition at finite temperatures. Two types of surface phases can be roughly identified; one is the hydrogen-rich phase that occurs at low temperatures, and another is the carbon-rich phase at high temperatures. For Ru, the adsorbed H atoms disappear above 650 K. Further increasing the temperature one would expect graphitization that eventually poisons the surface.[40] Therefore, a nondiminishing H coverage sets the high-temperature limit of a working FT catalyst. For Rh, we do not observe a sharp phase change, but the catalysts already have too low hydrogen coverage above 720 K. On the other hand, the low-temperature limit should largely be dictated by the CO dissociation ability, which can not be directly obtained from an equilibrium MC simulation.

As the stepped B_5 sites are the active site for CO dissociation, we have studied CO dissociation at the steps under various surface composition conditions. Obviously, a valid B_5 site for CO dissociation must have three connective vacant sites from the upper to middle and to the lower step (see Figure 6). CO initially adsorbs at a vacancy of the lower step and then dissociates by leaning down the O-end to the upper step. The whole CO dissociation process should be affected once the neighboring sites are covered by H and CH_x. We listed a set of calculated energy barriers of CO dissociation on Ru and Rh with and without coadsorbates in Figure 6.

In general, Ru catalysts are much more active than Rh in a CO dissociation. On the clean steps, the energy barrier of CO dissociation on Ru is 0.69 eV lower than that on Rh. In the circumstance that the middle steps are occupied by C or CH, we found that CO dissociation on Rh becomes unlikely with the energy barrier being more than 2.1 eV. The coadsorbed H atoms have only small effects on the energy barriers in general. Moreover, it is interesting to note that the adsorbates like CH at the neighboring upper step can decrease the CO dissociation barrier on Ru slightly but increase the barrier by 0.1 eV on Rh. To estimate the rate of CO dissociation, we next counted the number of valid B_5 sites from our MC simulations. We selected two kinds of B_5 sites that have the ability to dissociate CO. In the first type, there are no CH_x intermediates beside a three-connective-vacant B_5 site; in the second, only the upper step has neighboring CH_x intermediates. The other B_5 sites would either be too few in statistics or be too high in energy barriers for CO dissociation, so as that their contributions to the total CO dissociation rate are less than 1%. With the calculated energy barriers and the number of valid B_5 sites, we have estimated the rates of CO dissociation on Ru and Rh at various temperatures, which are drawn in Figure 7.

Figure 7 shows that Ru is ~4 orders of magnitude more active than Rh in dissociating CO. The CO dissociation rate on Ru exceeds 1 above 530 K so that it starts to be active at much lower temperatures than Rh (At very low temperatures (e.g., below 450 K); however, the Ru surface will be H-rich (Figure 3) and thus not efficient to catalyze C/C coupling for FT synthesis, shown later in section 3.5). Moreover, Ru can maintain good activity in a wider temperature window compared to Rh. This is because the number of active B_5 sites decrease sharply on Rh, since CO dissociation is strongly hindered if the middle steps start to be occupied by C or CH. In fact, the half-occupation of the middle steps by C or CH will totally block CO dissociation on Rh.

3.5. C/C Coupling of Chain Growth Reactions. The rate of C/C coupling reactions is the key to the selectivity of the FT process. Similar to the above approach to estimate the CO dissociation rate, we have searched for the reaction paths of all the possible C/C coupling reactions between CH_x intermediates on Ru and Rh surfaces, including both the terraces and the steps. The energy barriers of them at low coverages (without coadsorbates) are listed in Table 3, and the calculated TS structures are shown in the Supporting Information. As a reaction of A coupling with B over surface steps can have different transition state configurations, without specifically mentioning, we denote a reaction as A + B when the reactant A is from the upper step and B is at the lower step hereafter. Table 3 shows that steps are generally more active for C/C coupling than terraces. This also implies that FT reactions on Ru and Rh are structure

(40) Helveg, S.; Lopez-Cartes, C.; Sehested, J.; Clausen, B. S.; Rostrup-Neilsen, Jr.; Abild-Pedersen, F.; Norskov, J. K. *Nature* **2005**, *6973*, 427.

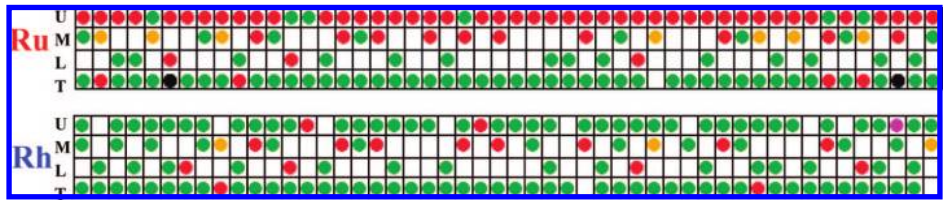

Figure 5. Equilibrium snapshots of Ru and Rh surfaces at 630 K from MC simulation. U, M, L, and T stand for the upper-step, middle-step, lower-step, and terrace sites, respectively (also see Figure 1). Green, H; yellow, C; red, CH; black, CH_2; purple, CH_3

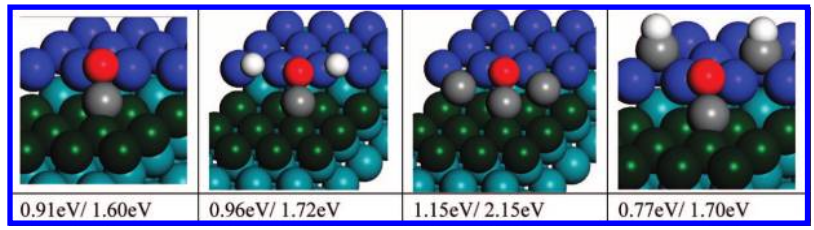

Figure 6. . Calculated reaction barriers and the transition state snapshots of CO dissociation with and without coadsorbates. The reaction barriers beneath the figures are for Ru and Rh, respectively.

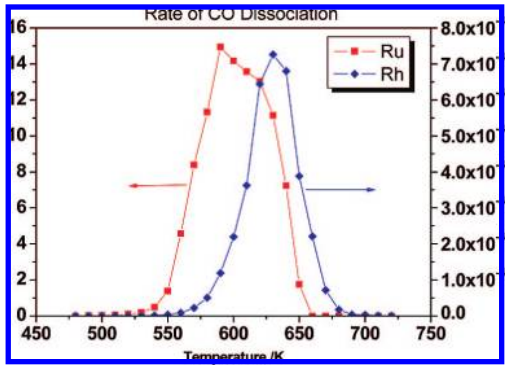

Figure 7. . Calculated rate of CO dissociation on Ru and Rh at various temperatures

Table 3. Calculated Reaction Barriers of C/C Coupling Reactions

terraces	Ru	Rh		Ru	Rh
C + CH	1.53	1.33	CH_2 + CH_2	1.27	1.34
C + CH_2	1.73	1.55	C + CH_3	1.18	1.00
CH + CH	1.07	1.42	CH + CH_3	1.35	1.19
CH + CH_2	1.23	1.46	CH_2 + CH_3	1.21	1.20

steps[a]	Ru	Rh		Ru	Rh
C + C	1.14	1.17	CH_2 + CH	1.21	1.34
CH + C	**0.72**	**0.94**	**CH_2 + CH_2**	**0.85**	**0.95**
C + CH	1.29	1.34	CH_3 + C	1.14	1.08
CH + CH	1.01	1.22	CH_3 + CH	1.37	1.61
CH_2 + C	1.33	1.56	CH_3 + CH_2	1.54	1.53

[a] For the reaction A + B occurring at steps, A is from the upper step and B is at the lower step except for the CH_2 + CH_2 reaction where both CH_2 adsorb at the step-edge.

sensitive,[18] which are in agreement with experimental observations.[41–43] It is noticed that on both Ru and Rh the lowest barrier channels of C/C coupling are via the CH + C and CH_2 + CH_2 reactions that happen at the steps. The reaction barriers of the two reactions on Ru are about 0.1−0.2 eV lower than those on Rh.

By taking into account the results from MC simulation, in particular the available types of C/C pairs together with their neighboring environments (the coadsorbates), we can have a close look on the C/C couplings reactions at more realistic conditions. For the CH + C reaction that has the lowest barrier at low coverages, such a combination indeed appears in the MC simulation but the neighboring middle steps are often occupied by H at low temperatures and CH or C at high temperatures. It therefore prompts us to further evaluate the influence of the middle-step coadsorbates. In CO dissociation, we already found that H atoms have less influence on the energy barriers than CH_x intermediates. Thus, we focused on the effects of coadsorbed C and CH. Taking the CH + C reaction on Ru as the example, we explicitly calculated the reaction barriers in the presence of CH−C, C−C, and CH−CH neighbors, and the results are shown in Figure 8, where the TS snapshots are illustrated. We found that these neighboring adsorbates can consistently reduce the reaction barrier by ∼0.2 eV, no matter whether the coadsorbates are C or CH. This may not be surprising as the coadsorbates mainly destabilize the initial state and the transition state through the surface-mediated bonding competition effect,[38,37,32] which are in a range of a few tenths of an electronvolt by itself (see Figure 2) and thus the difference between CH and C in their effects on reaction barriers should be even smaller.

Since the reaction barrier is not sensitive to the detailed neighboring environment being C or CH, we have calculated the reaction barriers of four important C/C coupling reactions by using the neighboring environment that is statistically most likely in MC simulations. For Ru, the neighbors are two C at the middle steps and two CH at the upper steps. As for Rh, there are also two C at the middle steps and hydrogen atoms at the upper steps. As coadsorbed hydrogens have little influence on the adsorption of C or CH, their effects on the association barriers were omitted. These calculated barriers are listed in Table 4. Importantly, our results show that under the more realistic conditions Ru and Rh have only marginal differences in the respect of the reaction barrier of C/C coupling. The lowest barrier on Ru is 0.57 eV, while it is 0.63 eV on Rh.

Now we can address the suitable temperatures for long-chain hydrocarbon production. As shown in Figures 3 and 4, the coverages of CH_x intermediates grow quickly on the surface with the increase of temperature. Therefore, the number of possible C/C pairs is generally higher at high temperatures. The

(41) Abrevaya, H; Cohn, H. M.; Targos, W. M.; Robota, H. J. *Catal. Lett.* **1990**, *7*, 183.
(42) Ojeda, M.; Rojas, S.; Boutonnet, M; Pérez-Alonso, F. J.; Garcia-Garcia, F. J.; Fierro, J. L. G. *Appl. Catal., A* **2004**, *274*, 33.
(43) Boudart, M.; McDonald, M. A. *J. Phys. Chem. B* **1984**, *88*, 2158.

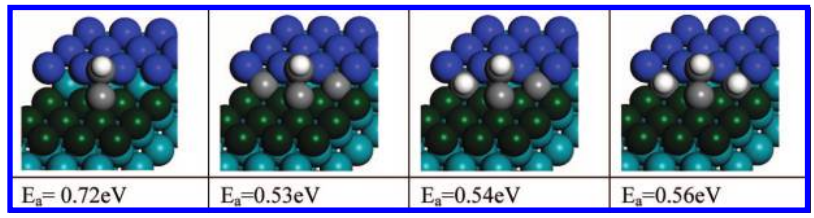

Figure 8. Reaction barriers of the CH + C reaction with and without coadsorbates at Ru middle steps.

Table 4. Reaction Barriers (Unit: eV) of Four C/C Coupling Reactions in the Presence of Coadsorbates (See Text for Details)

	CH + CH	C + CH	CH + C	C + C
Ru	1.21	1.48	0.57	1.33
Rh	1.11	1.00	0.63	0.64

Table 5. Rate of C/C Coupling Reactions at 630 K[a]

reactions	rate constants/s^{-1}	coverage of C/C pairs/ML	rate/ML·s^{-1}
Ru: CH + CH	6.53×10^{3}	4.80×10^{-3}	30.8
C + CH	49.2	$<5 \times 10^{-11}$	$<2.5 \times 10^{-9}$
CH + C	7.03×10^{8}	9.95×10^{-6}	$\mathbf{7.0 \times 10^{3}}$
C + C	3.30	$<5 \times 10^{-11}$	$<1.7 \times 10^{-10}$
$CH_2 + CH_2$	4.42×10^{6}	$<5 \times 10^{-11}$	$<2.2 \times 10^{-4}$
CH_2 + CH	4387	$<5 \times 10^{-11}$	$<2.2 \times 10^{-7}$
CH_3 +CH	25.2	$<5 \times 10^{-11}$	$<1.3 \times 10^{-9}$
Rh: CH + CH	3.99×10^{4}	8.30×10^{-4}	33
C + CH	2.92×10^{5}	1.56×10^{-7}	4.5×10^{-2}
CH + C	2.37×10^{8}	6.15×10^{-4}	$\mathbf{1.5 \times 10^{2}}$
C + C	1.98×10^{8}	$<5 \times 10^{-11}$	$<7.4 \times 10^{-3}$
$CH_2 + CH_2$	7.23×10^{5}	$<5 \times 10^{-11}$	$<3.6 \times 10^{-5}$
CH_2 + CH	400	$<5 \times 10^{-11}$	$<2 \times 10^{-8}$
CH_3 +CH	2.76	$<5 \times 10^{-11}$	$<1.4 \times 10^{-10}$

[a] The detection limit for the lowest coverage in our MC simulation is 5×10^{-11} ML, which is related to the total sampling point.

high temperature will also lead to the accumulation of the C and CH in the middle steps, which helps to reduce the C/C coupling reaction barriers (Figure 8). By considering the rate of CO dissociation that peaks at ~630 K for Rh, we choose 630 K to further examine the C/C coupling reaction. For comparison, we also take 630 K as the working temperature of Ru since Ru shows good CO dissociation activity in a wide range of temperatures. The typical surface compositions at 630 K for Ru and Rh have been shown in Figure 5.

We can then compare the rate of all possible C/C coupling reactions. Table 5 summarizes our calculated rate constants, the coverage of C/C pairs, and the calculated C_2 formation rate of selected C/C coupling reactions at 630 K. The other C/C coupling reactions not shown are unlikely to occur due to either too high reaction barriers or too low concentrations of reactants. At 630 K, Ru has more CH−C pairs than Rh and thus shows a greater rate of C/C coupling. This is due to the fact that Ru has a larger coverage of CH at the upper steps than Rh at 630 K (see Figure 5). Although Rh could have more CH−C pairs at higher temperatures in principle, its CO dissociation becomes too slow due to the C accumulation at the middle steps.

For Ru, our results show clearly that the CH + C is the dominant C/C coupling channel. This is consistent with our previous model,[18] where a CR + C coupling mechanism occurring over surface steps was proposed for chain propagation on Ru. However, Rh appears to have a second chain growth channel in addition to the CR + C channel. On Rh steps, the CH + CH reaction rate is comparable to that of the CH + C reaction. To further verify the chain growth possibility with a CR + CR (R = alkyl or H) mechanism, we have examined three prototypical reactions on clean Rh steps for C_3 formation,

Table 6. Calculated Rates of Hydrogenation Reactions at 630 K

	coverage of the pair (ML)	E_a (eV)	rate (ML·s^{-1})
Ru: C + H	1.02×10^{-2}	0.75	2.20×10^{4}
CH + H	0.329	0.56	2.32×10^{8}
CH_2 + H	3.66×10^{-5}	0.47	2.68×10^{7}
CH_3 + H	2.01×10^{-3}	1.06	**140**
Rh: C + H	3.54×10^{-2}	0.94	2.30×10^{4}
CH + H	0.160	0.70	8.55×10^{6}
CH_2 + H	8.27×10^{-5}	0.61	2.29×10^{4}
CH_3 + H	2.38×10^{-3}	0.74	6.00×10^{4}

namely CH + CCH_3, CCH_3 + CH, and CCH_3 + CCH_3. The reaction barriers are calculated to be 1.73 eV (CH + CCH_3), 1.21 eV (CCH_3 + CH), and 2.08 eV (CCH_3 + CCH_3), respectively. The reaction barriers of the CH + CCH_3 and CCH_3 + CCH_3 reactions are much too high, but CCH_3 + CH has a barrier comparable to that of CH + CH. Therefore, we expect that both CR + CH and CR + C pathways over Rh steps may account for the chain growth on Rh catalysts.

3.6. Hydrogenations. The methane production is the major competition route to chain growth. From a theoretical point of view, our grand canonical MC simulation assumes that the CH_x hydrogenation reactions are much faster than the C/C coupling reaction. This should be a valid assumption for a poor FT catalyst such as Rh but might be problematic for Ru where the C/C coupling rate may be comparable to the methane formation rate in reality. The assumption however can be checked by estimating the hydrogenation rates based on the rate equation according to the determined surface compositions and the calculated reaction barriers.

Similar to our analyses for C/C coupling reactions, we first calculated the reaction barriers of all hydrogenation reactions involving CH_x on Ru and Rh terraces. Our hydrogenation barriers are generally in good agreement (around 0.1 eV) with those reported previously[44] in view of different calculation setups (e.g., unit cell and basis sets). It was known that the hydrogenation reactions (methanation process) are structure-insensitive[39] and the reaction barriers of hydrogenations occurring on steps differ marginally from those on terraces.[7,45] Therefore, we used the barriers from the terrace to approximate the barriers of the hydrogenation reactions at different surface sites. Next, we counted the number of neighboring CH_x−H pairs at equilibrium at 630 K from MC simulation. The rates of hydrogenation reactions can then be worked out similarly as those for C/C coupling reactions, which are listed in Table 6, together with the calculated barriers.

The results clearly show that on Rh the hydrogenation reactions are indeed much faster (2 orders of magnitude) than the C/C coupling reactions (Table 5), where the slowest hydrogenation reaction occurs at the C + H and the CH_2 + H reactions. For Ru, the slowest step of hydrogenation occurs at the CH_3 + H step, which is about 50 times slower than the CH + C reaction. These results are consistent with the experimental

(44) Bunnik, B. S.; Kramer, G. J. *J. Catal.* **2006**, *242*, 309.
(45) Zhang, C. J.; Liu, Z.-P.; Hu, P. *J. Chem. Phys.* **2001**, *115*, 609.

observation that Ru selectively produces long-chain hydrocarbons, while Rh dominantly produces methane.[1,2] Since the CH + C reaction can not be neglected when treating the CH_x equilibrium on Ru, our grand canonical MC simulations here can only provide a qualitative picture of surface composition for Ru. We expect that there is a significant coverage of long-chain hydrocarbons (e.g., CR) on Ru at working conditions.

4. Discussions

4.1. Origin of the Selectivity Difference between Ru and Rh. We are now at the position to discuss what the most important factor is to the selectivity of FT conversion. By comparing the differences between Ru and Rh at working conditions, we may focus on the following four aspects.

(i) The surface composition at the steps. Our calculated adsorption energies show that the surface steps bond CH_x more strongly than the terraces and the potential energy surface of H is relatively flat. This implies that the stepped sites play a catalytic role to accumulate CH_x fragaments, as confirmed by the MC simulations. Although, at 630 K the terraces of both catalysts are still in a hydrogen-rich condition, the surface compositions at the steps are distinct. For Ru, the CH is highly populated at the upper step, which is the precursor for the C/C coupling reaction via the CH + C channel. The higher concentration of the CH−C pairs on Ru helps to increase the rate of C/C coupling. By contrast, the upper steps of Rh remain to be dominated by H atoms at 630 K. The C and CH species mainly accumulate at the middle step of Rh, which are however not the precursor for C/C coupling. This difference between Ru and Rh can be attributed to the potential energy surface of C and CH on the two surfaces. As shown in Table 1, the largest ΔE(t−s) on Ru occurs at the CH migrating from terraces to the upper steps, while that on Rh is the C moving to the middle steps.

(ii) The reaction barrier of C/C coupling reactions. Our DFT results show that there are little differences in the reaction barriers of C/C coupling reactions under realistic conditions. Both Ru and Rh can catalyze efficiently the coupling of two C_1 species with the reaction barriers at ∼0.6 eV. It should be emphasized that the lowest C/C coupling reaction barrier is generally lower than the highest reaction barrier of the hydrogenation steps (∼1 eV), even for the poor FT catalyst Rh.

(iii) The rate of hydrogenation reactions leading to methane. Our results show that Rh is more efficient than Ru in converting C_1 species to methane at 630 K. The slowest hydrogenation steps on Rh are the C + H and the CH_2 + H steps, which are, however, still 2 orders of magnitude faster than the slowest step, the CH_3 + H reaction on Ru. The reason for this is twofold. First, the CH_3 + H reaction on Ru has a higher reaction barrier, and second, the CH_3 coverage on the surface is intrinsically low compared to H, C, and CH species. For Rh, the high hydrogenation barrier and the low coverage do not occur at the same hydrogenation step, which leads to a general high rate of hydrogenation.

(iv) The CO dissociation activity. This is attributed to the most obvious difference between Ru and Rh. Since the stepped sites will accumulate CH_x species and help to grow long-chain hydrocarbons, it is essential that CO dissociation will not compete with the C/C coupling reactions for these sites. Ru remains to be efficient in catalyzing CO dissociation even when the stepped sites have high coverages of C_1 intermediates. However, Rh loses its CO dissociation ability quickly as the stepped sites start to be populated with C or CH species. This fact leads to Rh can either exhibit higher activity to yield methane or have lower activity but higher selectivity toward long-chain hydrocarbons.

To recap, the good FT catalyst must first be able to dissociate CO efficiently in carbon-rich conditions as Ru does. The carbon-rich conditions are reached first at surface steps, where the CO dissociation and the C/C coupling occur. Second, we also show that the calculated potential energy surface change from terraces to steps provides a convenient benchmark to predict whether the stepped sites can facilitate the accumulation of CH−C pairs. Third, the hydrogenation reactions may also be important. To improve the selectivity to long-chain hydrocarbons, it is better to have the high barriers in the CH_2 + H or CH_3 + H hydrogenation steps because CH_2 and CH_3 are much less populated on the surface than C and CH. At the moment, it may still be too early to judge whether these three factors are actually coupled with each other. Nevertheless, they constitute a useful guideline to design new FT catalysts in the future.

4.2. Chain Propagation Mechanism. Regarding the chain growth mechanism, we show that the CH + C pathway that occurs at surface steps is the most important C/C coupling channel on both Ru and Rh. This confirms our previously proposed CR + C chain propagation mechanism.[18] On Rh, an additional pathway involving CR + CH may also contribute to chain growth despite the fact that the total C/C coupling rate on Rh is much lower than that on Ru. Together with the MC simulations, we are able to rule out the other C/C coupling possibilities, for example, those involving CH_2 as the building monomer. The stepwise polymerization with methylene as the building monomer was first proposed by Brady in the early 1980s, and Maitlis and co-workers have developed this mechanism considerably by using isotope-labeling experiments.[12,46–49] They noticed that FT synthesis bears great similarity with the organometallic chemistry in the synthesis of long-chain hydrocarbons. However, the mechanism involving a CH_2 + CH_2R elementary step for chain propagation is not supported by theory. From our work, CH_2 is rare compared to C and CH on both surfaces due to its thermodynamic instability. The possibility for a CH_2 to meet a CH_2 or a CH_3 on the surface is extremely low. In addition to the thermodynamics, the CH_2 + CH_2 and CH_2 + CH_3 pathways also have much larger reaction barriers than that of the most efficient CH + C pathway. Even though the extra methylene species may be added from probing molecules such as CH_2Br_2 in experiments, it is highly likely that these CH_2 species will undergo decomposition to CH or C first and then take part in the chain propagation.

It might also be interesting to mention the experimental finding by Maitlis[49] that different propene isotopomers, $^{13}CH_2{=}{}^{13}CHCH_3$ and $CH_2{=}{}^{13}CH^{13}CH_3$, are present when the isotope-labeled $^{13}CH_2{=}{}^{13}CH_2$ are used as the probe molecule. This finding seems unexpected according to our CR + C mechanism that implies the double bond of α-olefin appears at the end of the newly arrived C_1 species. However, this may be explained as a result of the double-bond shift of the intermediates such as $CH{=}CHCH_3$. We suggest that the newly formed $C{-}CCH_3$ species can be hydrogenated to an intermediate $CH{=}CHCH_3$ (may lead to propene). The $CH{=}CHCH_3$ can undergo isomerization to shift its double bond to $CH_2{-}CH{=}CH_2$. The occurrence of the 1,3 double bond shift was already suggested by Maitlis in their chain growth mechanism.[47]

(46) Maitlis, P. M.; Quyoum, R.; Long, H. C.; Turner, M. L. *Appl. Catal., A* **1999**, *186*, 363.
(47) Quyoum, R.; Berdini, V.; Turner, M. L.; Long, H. C.; Maitlis, P. M. *J. Catal.* **1998**, *173*, 355.
(48) Maitlis, P. M. *J. Organomet. Chem.* **2004**, *689*, 4366.
(49) Turner, M. L.; Byers, P. K.; Long, H. C.; Maitlis, P. M. *J. Am. Chem. Soc.* **1993**, *115*, 4417.

While this paper is in revision, two interesting works on the FT mechanism were published. We felt obliged to discuss these results in the context of our new findings. King and the coworkers performed DFT calculations for CO hydrogenation on the Co{0001} surface.[50] They found that CO may not dissociate on Co{0001} but follows the sequential hydrogenation to form CH_2O and then undergoes C−O bond breaking to generate CH_x species. Although the surface investigated is different and the mechanism may not be transferable to Ru and Rh, we would like to point out that the new mechanism does not interfere with the grand canonical MC equilibrium of H and CH_x species on surfaces. Our calculated rates for C/C coupling reactions are therefore valid at any particular temperature. It is highly possible, however, that this new CH_x generation pathway, if present, in addition to CO dissociation will shift our determined working temperature range for a real FT catalyst. This may contribute to improving the chain growth ability for Rh at more carbon-rich conditions. But, since our results are consistent with the FT experimental facts on Ru and Rh, we believe that such additional effects may not be dramatic.

Maitalis and Zanotti recently proposed a new FT chain-growth mechanism via an RCH + CH pathway involving electrophilic CH as the building monomer.[51] Ciobica et al.[14] proposed two similar RCH + CH and RCH_2 + CH mechanisms earlier based on their DFT calculations on the Ru{0001} surface. Maitalis's new mechanism is deduced from an analogy of organometallic reactions and takes into account the fact of the high stability of CH on surfaces. From our chain growth mechanism, we agree with Maitalis that the CR (CH-like), CHR, and its 1,2 H shift isomer 1-alkene are most likely to be the key surface intermediates in forming long-chain hydrocarbons. However, it should be mentioned that we did not find the RCH + CH and RCH_2 + CH mechanisms to be feasible on Ru and Rh. The C/C coupling rates of these two paths via the CH_2 + CH or CH_3 + CH reaction are several orders slower than that of the CH + C reaction (Table 5). Second, the presence of positively charged CH species on metal surfaces is questionable, although Maitalis suggested the presence of positively charged CH carrier is the key for the chain growth in their organometallic reactions. This is because Fermi electrons of metals can easily quench any positive ions or radicals by transferring electrons from the surface to the electronegative adsorbates. The adsorbed fragments, H and CH_x, are always electron rich and covalently bonded with surface d-states.[37] Indeed, we notice that some evidence presented by Maitlis and Zanotti in support of their new mechanism involves materials such as titania, oxidized rohodium, which are not purely metals. We suggest that supporting metals on active oxides may well help to improve the CO dissociation ability at carbon-rich conditions by opening new C_1 generation channels (via CO dissociation or CO hydrogenation[50]) and thus enhance FT activity.

(50) Inderwildi, O. R.; Jenkins, S. J.; King, D. A. *J. Phys. Chem. B* **2008**, *112*, 1305.
(51) Maitlis, P. M.; Zanotti, V. *Catal. Lett.* **2008**, *122*, 80.

5. Conclusions

In summary, this work presents the first detailed study on Fischer−Tropsch synthesis over Ru and Rh by combining first-principles calculations with grand canonical Monte Carlo simulations. We developed a two-dimensional Monte Carlo model to describe the chemistry of surface steps, consisting of both stepped sites and terrace sites. Based on the equilibrium conditions achieved by Monte Carlo simulations, we have studied CO dissociation, C/C coupling, and hydrogenations under more realistic catalytic conditions.

Our main conclusions are outlined as follows. CH and C are found to be the dominant C_1 intermediates on surfaces. Chain growth is unlikely to involve CH_2 for both thermodynamics and kinetics. The CR + C mechanism previously proposed for chain propagation on Ru may well be a general chain propagation mechanism for other metals. For the poor FT catalyst such as Rh, a second mechanism CR + CH may also be operative owing to the overall low rate of chain growth. We emphasize that it is vital that a good FT catalyst must be active for CO dissociation when the stepped sites are in carbon-rich conditions. The surface defects such as steps facilitate the accumulation of CH_x species, which is the key to growing long-chain hydrocarbons. The FT process thus should be structure sensitive. In addition to the CO dissociation ability, the potential energy surface of CH and the hydrogenation barriers of CH_2 + H and CH_3 + H are the other two key factors that influence the selectivity of the FT process.

Acknowledgment. This work is supported by NSF of China (20573023, 20773026, 20721063), Pujiang plan, NSF of Shanghai Sci. Tech. Committee (06PJ14011). Shanghai Supercomputing Center is thanked for computing time. Jia Chen acknowledges Dr. Chuang-Ming Wang and Mr. Chong Liu for stimulating discussions and kind instructions in computations.

Supporting Information Available: The transition state structures of all calculated C/C coupling reactions, the xyz coordinates and the absolute energies of all important structures. This information is available free of charge via the Internet at http://pubs.acs.org/

JA7112239